J. Fluid Mech. (1984), *vol.* 144, *pp.* 79–101
Printed in Great Britain

Laminar boundary-layer transition on a heated underwater body

By GERALD C. LAUCHLE AND G. B. GURNEY
The Pennsylvania State University, Applied Research Laboratory, Post Office Box 30, State College, PA 16804

(Received 7 November 1983)

A large (3.05 m long × 0.32 m diameter) heated-surface, axisymmetric body, designed for transition research in a 1.22 m diameter water tunnel is described. Boundary-layer transition data are presented as functions of the heating power supplied to the body and the total concentration of free-stream particulate matter in the water. Body surface temperatures range from 0 to 25 °C over the ambient water temperature, and the total heat supplied ranges from 0 to 93.3 kW. Transition-arclength Reynolds numbers are found to vary from 4.5×10^6 for the body operating cold to 3.64×10^7 for the maximum heat level considered. The concentration of free-stream particles is shown to affect the transition Reynolds number. These particles range in diameter from 10 to 70 μm and their concentration ranges from less than 5 to 198 particles per cm^3. The decrease in transition Reynolds number due to to the higher concentration of particles is of order 30 %.

1. Introduction

Early wind-tunnel experiments such as those of Frick & McCullough (1942) and Liepmann & Fila (1947) suggest that the transition location of a flat-plate boundary layer in air is moved forward as a result of surface heating. Because this effect is suspected to be due to the variation of fluid viscosity with temperature, it has long been speculated that the opposite effect would occur in water. In particular, the viscosity of water decreases with increasing temperature, which results in a viscosity gradient close to a heated wall. The lower viscosity near the wall would tend to promote larger velocities near the wall, which results in a fuller, more stable laminar velocity profile than the Blasius profile. Cooling in water (and heating in air) results in higher viscosity near the wall, which can lead to an inflected velocity profile, which is unstable.

Numerical calculations by Wazzan, Okamura & Smith (1968, 1970) confirm that wall heating can produce large increases in the transition Reynolds number of water boundary layers. In this analysis, the stability characteristics of the boundary layer are predicted from the solution of a modified fourth-order Orr–Sommerfeld equation. Lowell & Reshotko (1974) refined these predictions further by introducing a coupled sixth-order system of vorticity and energy disturbance equations. Such calculations have demonstrated that transition Reynolds numbers (based on free-stream velocity and distance from the leading edge of a flat plate) can reach as high as 2×10^8 for wall temperatures that are 40 °C above the water temperature. These analytical methods and others are thoroughly reviewed by Reshotko (1976).

From a practical point of view, the delaying of transition can result in significant drag reduction. Reshotko (1978) presents a series of calculations of skin-friction

reductions for a heated flat plate at zero incidence. These calculations account for the effectiveness of transmitting the reject heat from a propulsion system to the water in the desired manner. Even with a moderately efficient heat exchanger, drag reductions in excess of 60 % are possible at transition Reynolds numbers of the order of 7×10^7.

The potential payoff in drag reduction has triggered a fair amount of recent experimental research in heated laminar boundary-layer flows. Strazisar, Reshotko & Prahl (1977) present experimental results for the stability of an artificially excited laminar layer over a heated flat plate at zero incidence. For low wall overheats ($\Delta T = T_w - T_0 \approx 2.8$ °C, where $T_w \equiv$ wall temperature and $T_0 \equiv$ water temperature), they establish neutral stability curves from which critical Reynolds numbers can be determined. The results are in reasonable agreement with predictions. This work represents one of the first verifications of the predictions of Wazzan *et al.* (1968) and Lowell & Reshotko (1974).

The experiments of Strazisar *et al.* (1977) are limited to very low streamwise Reynolds numbers and overheats. Barker & Gile (1981) describe a series of heated-pipe experiments of which one of the goals is to explore the upper limits of transition Reynolds number through wall heating. Their experiments are conducted on the inside of a long (6.1 m), electrically heated pipe. Because the displacement thickness is thin relative to the pipe radius, the boundary-layer development is approximately the same as that of a zero-pressure-gradient flat plate. For a wall overheat of 8 °C, Barker & Gile measure a transition Reynolds number of 4.7×10^7. As the wall heating is increased further, these authors note that there is no further improvement in transition Reynolds number, which is in contradiction with theory. Barker & Gile attribute the observed limitations to flow asymmetries and free-stream particulates. The flow asymmetries originate in the entrance region of the pipe and are in the form of a large longitudinal vortex pair. Yao (1977) analyses this flow in the context of the flow-tube experiments and concludes that laminar instabilities will occur at high heating levels.

The effects of free-stream particulates on transition location are not at present very well understood, particularly for the very high Reynolds numbers associated with heated laminar flow. Ladd & Hendricks (1982) have initiated a quantification of these effects through tests on a small (50 mm diameter), 9:1 fineness ratio ellipsoid in a water tunnel. Their transition Reynolds numbers vary from 3.0×10^6 to 7.5×10^6, and the tunnel water is seeded with known concentrations of particles ranging from 12 to 133 μm in diameter. Overheats range from 0 to 15 °C. At the higher transition Reynolds numbers considered, Ladd & Hendricks conclude that the 80 and 133 μm particles have a degrading effect on transition Reynolds number. They estimate a critical particle Reynolds number (based on free-stream velocity and particle diameter) to be of order 700. It is pointed out that this critical Reynolds number does depend on heating level, surface finish, particle concentration and a judgment as to where the effect is important. Based on these results, it appears that free-stream particles have a detrimental effect on transition Reynolds number, but further work is necessary to identify the mechanisms by which particles destabilize the laminar layer. Chen, Goland & Reshotko (1979) give a qualitative analysis of particle/boundary-layer interaction, but the method does involve some empiricism. The authors remark that detailed experimental efforts are needed to utilize the analysis more fully.

The present investigation addresses the stability of the laminar layer over a relatively large, heated-surface underwater body. This body has been designed

specifically for transition research in the Garfield Thomas 1.22 m diameter water tunnel located at the Applied Research Laboratory on The Pennsylvania State University campus. Considerable engineering effort has been given to the design and manufacture of this body so that it can be a versatile tool for transition research. The body surface is heated electrically so that heating distributions can be changed within rather broad limits. The shape of the body is one that yields a mildly favourable pressure gradient along its length. The surface of this body is polished nickel, and is typical of 'best-effort' polishing by a skilled craftsman.

The water tunnel in which the heated body is tested is adequate for many laminar-flow experimental programs. Turbulence management includes both coarse- and fine-mesh honeycomb and a 9:1 contraction ratio settling section. The background noise is quite low owing to excellent cavitation performance of the impeller. The important feature of this facility is its high-unit-Reynolds-number capability. After heating of the water (48 °C), unit Reynolds numbers of 3.49×10^7/m can be achieved at a maximum water velocity of 19.8 m/s.

The transition data reported in this paper represent baseline data for the subject body. One objective is to estimate, theoretically, heat distributions for the body based on the analysis of Eisenhuth & Hoffman (1981) that should result in a stable boundary layer. These estimates are thence compared with the experimental findings. Another objective is to show qualitatively any dependence of transition Reynolds number on the concentration of free-stream particulates that are present in the water.

2. Experimental apparatus

2.1. *The 1.22 m diameter water tunnel*

The facility used in the current heated-body investigation is a closed-circuit low-turbulence water tunnel which has a test-section length of 4.27 m and a diameter of 1.22 m. A complete description of this facility is given by Lehman (1959).

The turbulence in the test section is quite low for a water tunnel of this size. The settling section contraction ratio is 9:1 and its upstream section contains a flow straightener and honeycomb. The flow straightener is a 0.61 m long square-mesh arrangement with a cell size of 10.16 cm. The stainless-steel honeycomb is situated 0.61 m downstream from the straightener, is 20.32 cm thick, and has an octagonal cell shape 0.56 cm from flat to flat. Lumley & McMahon (1967) describe the design considerations for this turbulence-management system. The longitudinal component of turbulence intensity in the test section and settling section has been measured and reported by Robbins (1978). Figure 1 shows the tubulence intensity as a function of test-section velocity. The higher levels below 8 m/s are suspected of being due to laminar instability within the cores of the honeycomb. The majority of the data presented in §4 are for velocities greater than 8 m/s, where the turbulence intensity is of order 0.1 % and the average integral length-scale is 1.25 cm. As shown by Lauchle, Eisenhuth & Gurney (1980), this level is sufficiently low for transition research.

A feature of the 1.22 m diameter water tunnel worth noting is its degassing and filtering capability. A fluid bypass system is available which is used to pass the water through 10 μm filters and deaeration modules. The maximum flow of this system is 190 l/s. The deaeration modules are small, plastic saddle-shaped units. Many thousands of these modules are contained in a large settling tank through which the water flows. The resulting trickle of water over the modules effectively removes dissolved and free gas. Particulate matter is removed by filters in this bypass system.

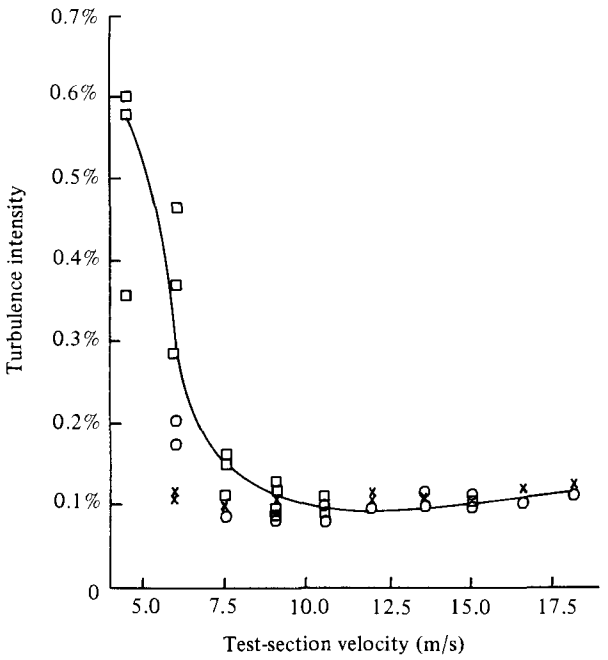

FIGURE 1. Test-section tubulence intensity as measured in the 1.22 m diameter water tunnel by Robbins (1978): ×, □, measured in the test section; ○, calculated from levels measured in the settling section.

The water temperature increases with time as the facility is operated. Typically, for a test-section velocity of 13 m/s, the temperature increases at a rate of 1 °C per hour. Testing at constant Reynolds number can be achieved by computer/tunnel operator interaction because water temperature, velocity, and pressure data are passed to an online VAX computer every 10s.

The water quality can be determined at any time during the course of a test. The dissolved gas content α_0 is measured with a Van Slyke apparatus. This instrument is primarily used in the medical diagnosis of blood, but can also be used for water. The net output is the number of moles of dissolved gas per total number of moles, expressed in parts per million (p.p.m.).

The free gas in the test section can be measured with a laser light-scattering system developed by Davis & Billet (1983). This system measures the number of bubbles per unit volume for each of seven different resolution channels ranging from 9 to 48 μm bubble diameter.

Water purity is determined by either of two methods. The one method, developed by Billet & Gates (1981), uses optical holography to sample statistically a volume of the tunnel water. Particle-size distributions covering the 10 to 70 μm mean diameter range can be determined with this system. The other method involves the passing of any selected volume of tunnel water through a Nuclepore membrane filter. Photomicrographs of the filter are produced using a Scanning electron microscope (SEM) located at the Materials Research Laboratory on The Pennsylvania State University campus. The photomicrograph is further scanned with the SEM and a statistical estimate of the size distribution of particles is performed. This system is capable of counting any size particle, but typically the measurements cover a 1–1000 μm mean diameter range.

2.2. *The heated body*

The body shape considered for this investigation is described mathematically by a family of modified ellipse functions. It is typical of the kind of underwater body whose transition location might be effectively delayed through use of surface heating. The equation that describes the body coordinates is given by

$$\hat{y} = [\hat{x}(2-\hat{x})]^{\frac{1}{2}} - K_n \frac{C_0 \hat{x}}{2a^2} \exp\left\{-\frac{\hat{x}^2}{2a^2} - kK_n\right\} + \hat{x}^2 \epsilon_L, \tag{1}$$

where $\hat{x} = x/l_n$, $l_n \equiv$ nose length, $\hat{y} = r_b/\frac{1}{2}D_{max}$, $D_{max} \equiv$ maximum diameter, $K_n = l_n/D_{max}$, $a = 0.3$, $C_0 = 0.0303$, and $k = 0.45227$. Here x is the axial coordinate and r_b is the body radius. The parameter

$$\epsilon_L = \frac{K_n C_0}{2a^2} \exp\left\{-\frac{1}{2a^2} - kK_n\right\}. \tag{2}$$

Equation (1) describes the shape from $x = 0$ to $x = l_n (l_n = 2.44$ m), where $r_b = \frac{1}{2}D_{max}$ ($D_{max} = 0.32$ m). From $x = l_n$ to $x = L (L \equiv$ total length $= 3.05$ m) the body fairs into a 0.2 m diameter sting. The fairing curve is a simple arc of radius 1.29 m combined with an inflexion curve at the sting juncture.

Calculations and measurements of the pressure distribution over this body are given by Lauchle (1979). The computed potential flow results are repeated here in figure 2. The calculations for the pressure coefficient C_p and pressure-gradient parameter β account for the solid blockage that occurs on bodies operating within the confines of tunnel walls. The parameter β is calculated in the standard way, i.e.

$$\beta = \frac{2M}{M+\lambda+1}, \tag{3}$$

where

$$M = \frac{x}{u_e}\frac{du_e}{dx}, \tag{4}$$

$u_e =$ edge velocity,

and

$$\lambda = \frac{2x}{r_b}\frac{dr_b}{dx}. \tag{5}$$

It is seen from figure 2 that this body supports a mildly favourable pressure gradient along most of its length. The parameter β remains relatively constant and positive, indicating that the pressure gradient is relatively constant and favorable.

Given the information contained in figure 2, temperature and heat-flux distributions can be predicted that should result in laminar flow over the body to the maximum-diameter point ($\hat{x} = 1$). These calculations are performed using the method of Eisenhuth & Hoffman (1981). (Note that the numerical examples given in this reference are for this particular body.) The method makes use of similarity solutions of the boundary-layer equations which include the heat-transfer terms, although transverse-curvature terms are neglected. The parametric procedure permits one to estimate heat distributions based on either of two criteria. The first criterion insures the maintenance of laminar flow by the addition of just enough heat to keep the local displacement thickness Reynolds number equal to the minimum critical Reynolds number established previously by Lowell & Reshotko (1974). This heating level is referred to as the 'minimum distribution'. The second criterion is based on the fact

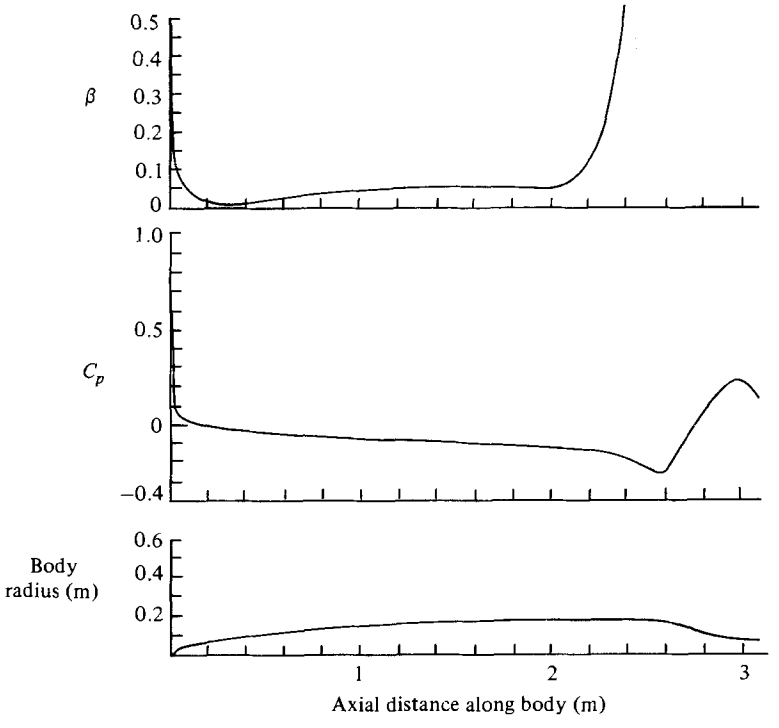

FIGURE 2. Potential-flow calculations of pressure coefficient and pressure-gradient parameter for the heated body including wall effects.

that there is a peak critical Reynolds number at about 65 °C overheat (Lowell & Reshotko 1974). Thus the method provides enough heat so that the peak critical Reynolds number is always maintained. This level of heating is referred to as the 'maximum distribution'. Heating above this level appears to provide less enhancement of the laminar-layer stability. The maximum-temperature distribution is independent of velocity, while the minimum distribution does change with the operating velocity. Because the local Reynolds numbers are equal to or less than a critical value, no amplification of spatial disturbances in the laminar layer would be expected. The results of these predictions will be discussed in §4.

The heating system for the test body is designed to provide enough heat so that a theoretical maximum-heat-flux distribution can be achieved with the tunnel operating at its maximum velocity of 19.8 m/s and typically high water temperature of 32.2 °C. In order to provide flexibility in the setting of given heating distributions, an electric heat exchanger is used in the body. This heat exchanger consists of 32 individually controlled axial heat zones. Figure 3 shows a cutaway view of the body construction. A typical heat zone is an aluminium ring, 7.62 cm in length and 2 cm thick. The ring is fitted with a dense array of commercially available cartridge heaters. The array of heaters are parallel wired and the common leads are connected to the power source and controller.

Each aluminium ring, or heat zone, is machine-fitted to its adjacent ring. When all rings are stacked together (several internal tie rods secure the assembly) an inner body of length l_n is formed. At first assembly this inner body was machine finished as a unit. It was then used as a mandrel for electroforming a solid nickel outer shell.

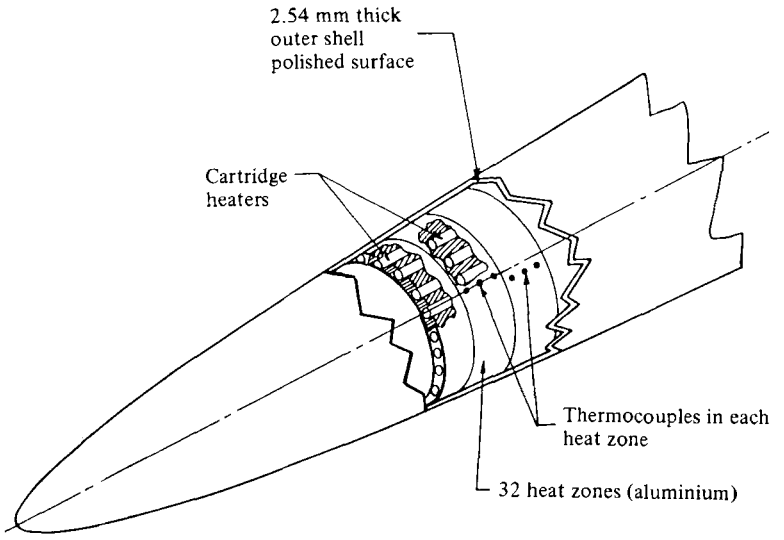

FIGURE 3. A schematic view of the heated body.

The electroformed nickel outer shell is 2.54 mm thick and 2.44 m long. Its surface is machined to the shape given by (1) using a numerically controlled lathe and then buffed and polished to a fine finish. Surface waviness is less than 25 μm in 10 cm, and the r.m.s. value of the random surface roughness is of order 0.5 μm.

The inner rings can be removed from the nickel shell for wiring or repair. When the body is reassembled, a thermally conductive, silver-impregnated grease is used between the inner body and outer shell. Register marks permit the body to be reassembled in exactly the same way it was during the electroforming process, thus minimizing misalignment, which would degrade heat transfer.

The heated nose portion of the body ($0 \leqslant x \leqslant l_n$) is secured to a stainless-steel afterbody and sting mount. Figure 4 shows a photograph of the body as installed in the 1.22 m diameter test section. The afterbody is equipped with a strain-gauged force balance for total-drag measurements. Because of certain unresolved problems with the balance, there will be no further discussion of drag measurements in this paper.

2.3. *Instrumentation*

The instrumentation used in the experimental programme includes the equipment necessary to measure body heat flux, body temperature, transition, water quality and operational parameters. Because the techniques for measuring water quality have been discussed in § 2.1, no further discussion is given here.

The operational parameters include test-section velocity u_0, ambient pressure P_0 and ambient water temperature T_0. Velocity is determined from the pressure drop between the settling section and the entrance of the test section. The ambient pressure is measured at the test section entrance. These pressures are determined using Validyne-AP-10 absolute and DP-15 differential pressure transducers. The water temperature is monitored in the settling section with an RTD sensor with digital output. All signals are passed through a 100 channel Data Systems multiplexer and then to a VAX digital computer system for subsequent conversion to engineering units. The multiplexer updates all readings every 10s.

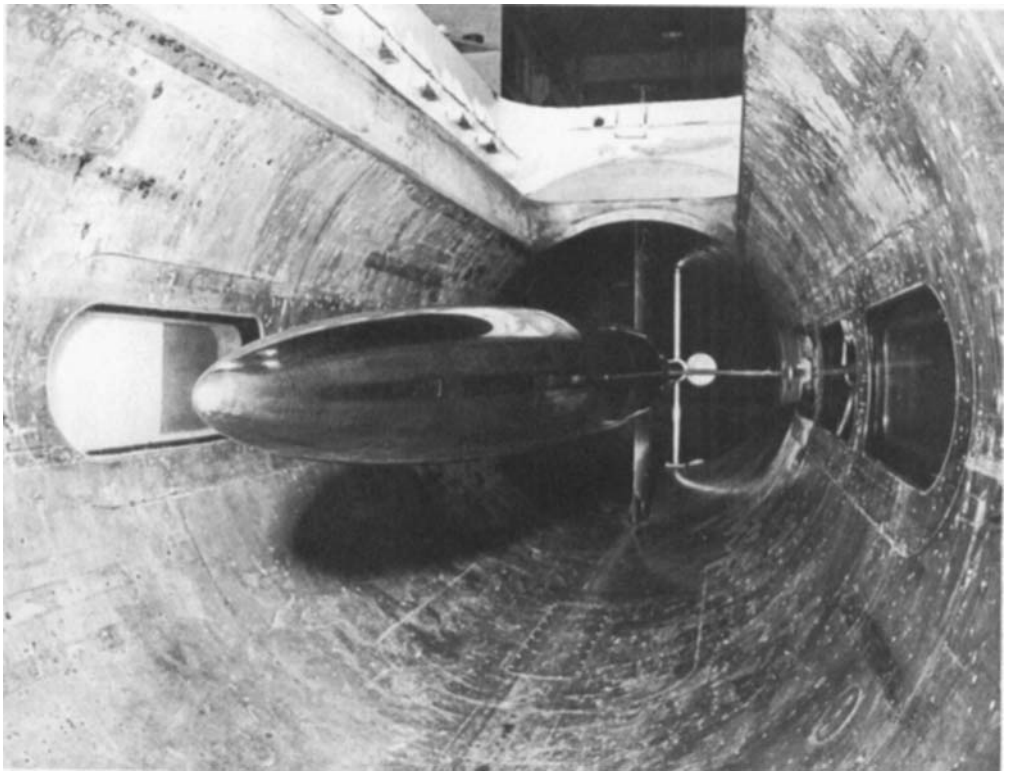

FIGURE 4. Photograph of the heated laminar-flow body in the 1.22 m diameter test section.

As noted in figure 3, each heat zone contains a group of thermocouples (typically four). These thermocouples are made from chromel/alumel, ANSI Type K wires. The junction is crimped using commercial nickel sleeves. The measurement junction is very close to the outside surface of the inner shell. A procedure for estimating wall temperature from measurements made at the inner/outer shell interface is discussed in §3. The 90 body thermocouples pass from the body to a copper zone box along with a thermocouple from an Omega Model TRC-III ice-point cell and then to the 100 channel multiplexer. The voltages are monitored with a H/P voltmeter and transmitted to the VAX computer. The wires are individually calibrated prior to installation; the conversion of voltage to temperature units being performed in the VAX computer. Cathode-ray-tube display of the body-temperature distribution is achieved in nearly real time. The accuracy of the temperature measurement system is estimated to be ± 0.5 °C.

Body heat-flux distributions are estimated from the ratio of the electrical power supplied to each of the 32 heat zones to the wetted surface area of the given zone. This procedure is most valid under the conditions of forced convection when the heat-flux vector is radially outward. It has been estimated (Stinebring 1977) that for the typical water velocities used, the ratio of outward heat flow to inward (toward centre of body) heat flow is of order 10^3. The electrical power of each zone is varied with custom-designed SCR-type controllers; each rated at 7.5 kW. The power can be adjusted in 1 % increments of the load.

A Magtrol digital power meter has been modified by General Electric Corp. to selectively monitor the power supplied to each heat zone. This device integrates the

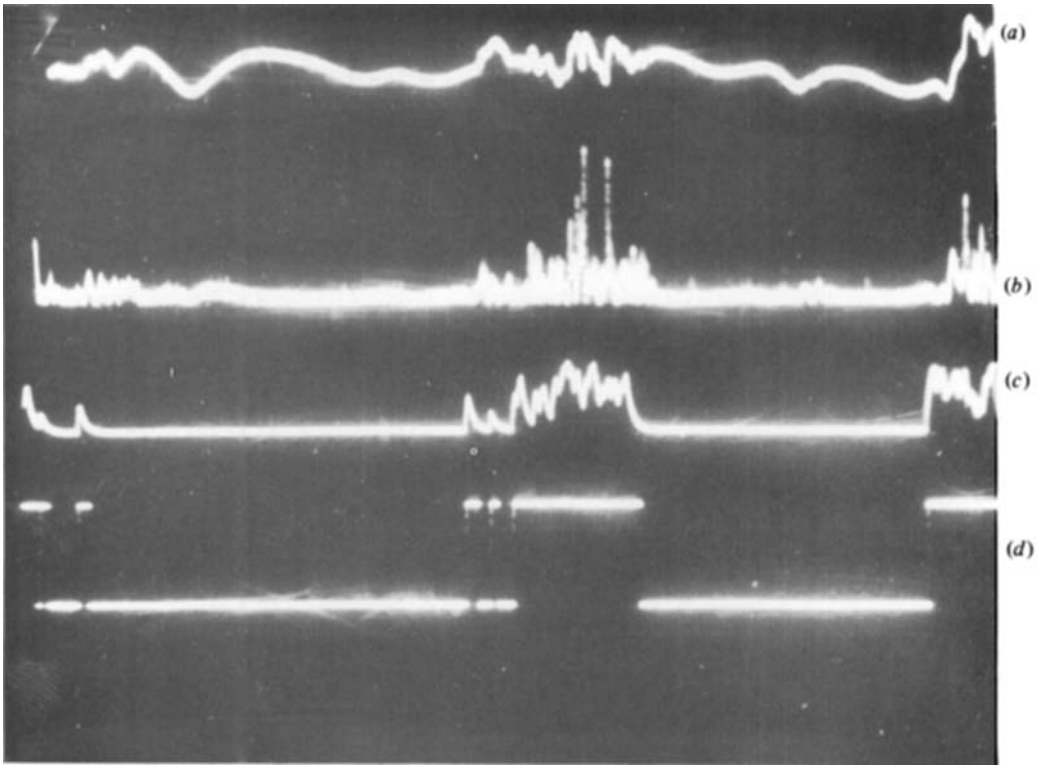

FIGURE 5. Oscilloscope traces showing: (*a*) hot-film signal; (*b*) signal (*a*) after differentiation and full-wave rectification; (*c*) signal (*b*) after low-pass filtering; (*d*) Schmidt trigger output (indicator function) after operation on signal (*c*).

product of voltage and amperage for a period of 30 s and displays the wattage digitally. The manufacturer of the power meter states the accuracy to be $\pm 0.25\,\%$ of the displayed reading. For the typical power levels used in this investigation, an estimated accuracy is of order ± 6 W.

In order to maintain a high-quality surface finish, the hot-film probes used for monitoring transition are not placed in the heated portions of the body. Rather, three flush-mounted films (TSI Model 1471) are spaced at 120° increments around the body at the downstream end of the last heat zone. The arclength distance s to the probes is 2.12 m. Consequently the arclength Reynolds number is measured for a fixed distance and is varied by varying the free-stream velocity. The hot-film signals are processed using standard DISA 55M01 anemometers and DISA 55D26 signal conditioners.

Transitional flow over a fixed hot-film probe is intermittent owing to the creation and convection of turbulent spots. This intermittent flow is described, statistically, by the intermittency factor γ and the burst-formation rate N. An indicator function $I(t)$ is defined as a zero–one function; it is zero if the boundary layer is laminar and it is one if the layer is turbulent. The factor γ is the time-average value of $I(t)$, and N is a count of the average number of step changes in $I(t)$ per unit time. An intermittency detector is used to generate $I(t)$. Its operation is as follows: (1) the hot-film signal is high-pass filtered to eliminate very-low-frequency components (typically set at 50 Hz); (2) the signal is differentiated and full-wave rectified so

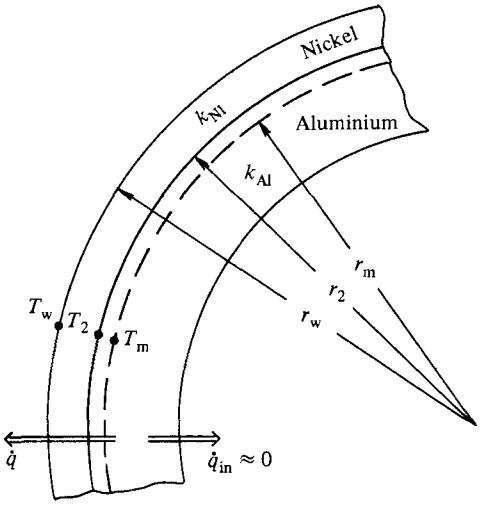

FIGURE 6. Definition of variables used in (6).

as to enhance high-frequency turbulent fluctuations, and be representative of a fluctuating vorticity signal (Taylor's frozen-vorticity assumption); (3) it is integrated with a short-time-constant low-pass filter in order to smooth the fluctuations within a burst; (4) the conditioned signal then passes through a Schmidt trigger with adjustable threshold. The output of the Schmidt trigger is $I(t)$. Figure 5 shows these steps as performed on a typical hot-film signal obtained in a transitioning boundary layer. The intermittency factor is determined by passing $I(t)$ through an integrating voltmeter, and N is established by passing $I(t)$ through a counter that triggers only on the leading edge of the unit step functions. Both quantities are determined for record lengths of 100s or more. As explained below, the value of γ is used to establish transition for these experiments.

3. Experimental procedures

The hot-film probes are used only for the detection of transition. Therefore an absolute calibration is not necessary. The intermittency detector is set up using a storage oscilloscope. The velocity is adjusted so that an approximately 50% intermittent signal is observed. The detector threshold voltage is adjusted until the indicator function tracks with the turbulence bursts sensed by the films. This setting is very rarely changed through the course of a test. This stability is attributed to the fact that the d.c. component of the film signal is removed by high-pass filtering.

The transition Reynolds number is determined from measurements of γ versus u_0. The velocity is set at a low value where $\gamma \approx 0$ (fully laminar flow over the hot-film probe). It is then increased incrementally and fixed while γ and N are established. After the higher velocities (where $\gamma = 1$) have been achieved, the sequence is repeated by decreasing u_0 in increments. The values of γ and N are also determined during the decreasing-velocity part of the run. It is again noted that 100 s (or more) of integration time is used for each datum. The abscissa is converted to arclength Reynolds number ($Re_s = u_0 s/\nu$, where ν is the kinematic viscosity determined for the water temperature at the time the datum is measured, and $s = 2.12$ m). The arclength Reynolds number at the point where $\gamma = 0.5$ is defined as the transition Reynolds

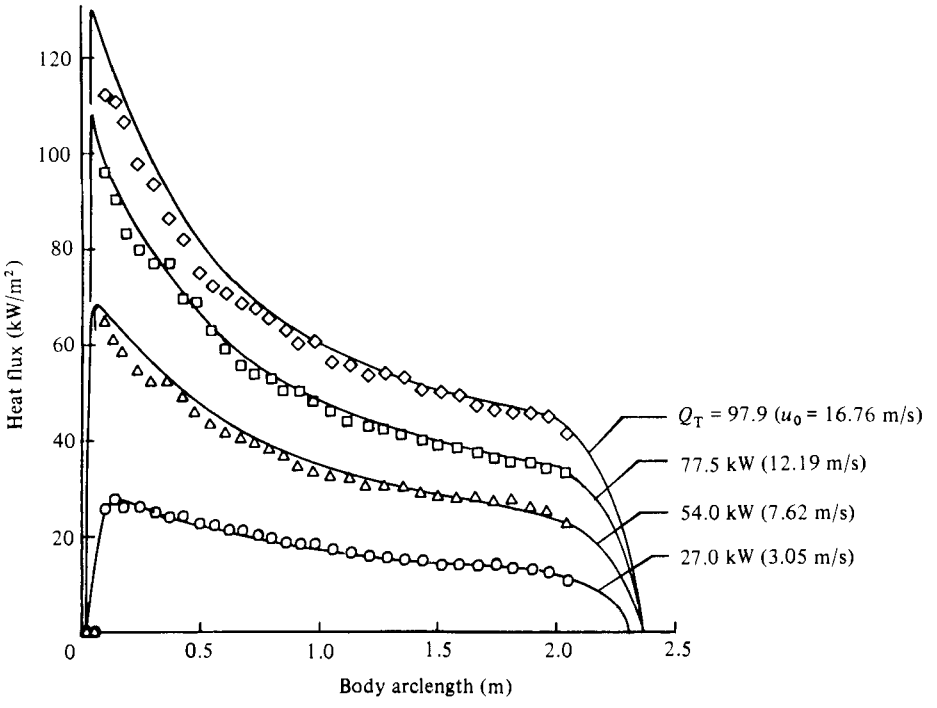

FIGURE 7. Predicted and measured heat-flux distributions for the heated body: —, theoretical predictions; ○, Q_T = 26.6 kW; △, 53.4 kW; □, 75.4 kW; ◇, 93.3 kW. T_0 = 25.6 °C (78 °F).

number. These numbers may be multiplied by 1.085 to obtain the arclength Reynolds number based on edge velocity u_e. This constant arises from the value of C_p at $s = 2.12$ m.

The heat-flux distributions are measured in a straightforward manner. As previously noted, the electrical power supplied to a given heat zone is simply divided by the wetted surface area of the zone. The procedure is approximate because of the small unknown amount of heat that leaks axially from zone to zone. No attempt has been made to account for this effect.

The surface or wall temperature T_w is estimated from the measured temperature T_m by an elementary method. Figure 6 shows a cross-section of the body in a plane containing a thermocouple. If $\dot{q}$ is the heat flux for the particular zone and l is the axial length of the zone then

$$T_w = T_m - \frac{\dot{q}}{2\pi l}\left[\frac{\ln (r_2/r_m)}{k_{Al}} + \frac{\ln (r_w/r_2)}{k_{Ni}}\right]. \tag{6}$$

The constants k_{Al} and k_{Ni} are the thermal conductivities of aluminium and nickel respectively. Equation (6) assumes a perfect contact at the aluminium/nickel interface and that the heat flux is predominantly radially outward.

Free-bubble distributions are measured with the light-scattering nucleii counter of Davis & Billet (1983). These measurements are performed in the test section near the maximum-diameter point of the body. Because bubble diameter is affected by dynamic pressure, these distributions are measured over a range of velocities. The tunnel pressure P_0 has been held constant at 241.3 kPa (absolute) for all data presented in this paper.

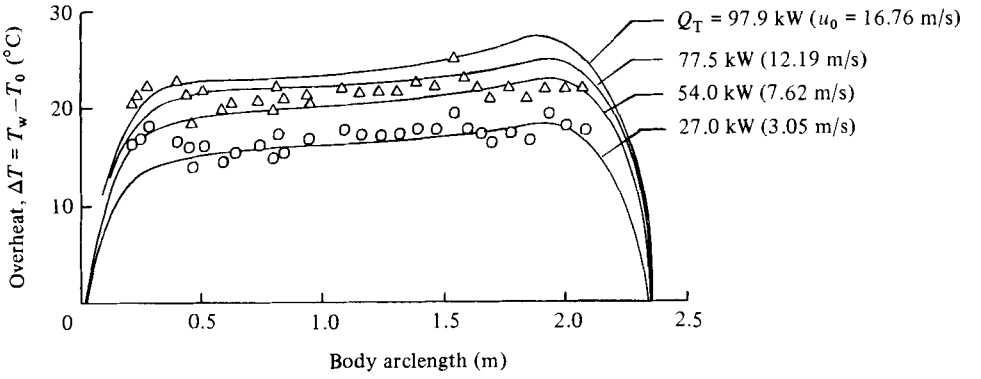

FIGURE 8. Predicted and measured wall-temperature distributions for the heated body: —, theoretical predictions; ○, measured at $Q_T = 26.6$ kW, $u_0 = 3.05$ m/s; △, $Q_T = 53.4$ kW, $u_0 = 7.62$ m/s. $T_0 = 25.6$ °C (78 °F).

The water samples used in determining particulate distributions are collected through a valve located on the bottom side of the settling section. Lauchle & Crust (1980) report that the measured distributions depend very little on free-stream velocity or pressure.

4. Results

4.1. *Heat distributions*

The heat distributions selected for experimental study are those minimum distributions calculated for $u_0 = 3.05$, 7.62, 12.19 and 16.76 m/s at a water temperature $T_0 = 25.6$ °C. As noted earlier, each of these distributions should provide enough heat to keep the boundary layer neutrally stable to the point of maximum diameter on the body at velocities less than or equal to the value quoted. The heat flux distributions are shown in figure 7, while the corresponding temperature distributions are given in figure 8. Integration of the heat-flux distribution over the wetted surface area of the body gives the total heating power supplied to the body. These integrated values are denoted by Q_T and are indicated on figures 7 and 8. In later discussions of the transition data, Q_T will be used as the parameter that identifies which distribution is being referred to. It is seen from figure 7 that the measured heat flux distributions agree well with the theoretical distributions.

The agreement between the measured wall temperature and that predicted is fair (figure 8). The temperature data shown are measured at the value of u_0 noted and under laminar-flow conditions. These data include the correction for skin thickness described by (6), in which measured values of $\dot{q}$ are used. The scatter in these data is attributable to the slight scatter in the heat-flux distributions and to the non-perfect contact between the inner and outer shells of the body.

Temperature data are not shown for the two highest heating conditions because the boundary layer was observed to be intermittent at the hot-film location. This intermittency greatly affects the heat-transfer characteristics of the body and results in random fluctuations of the wall temperature. Repeatable data could not be produced near the end of the body, where the layer is intermittent. Although not explored in detail, the thermocouple data can be used to indicate transition location. However, the axial resolution is poor when the intermittent flow regimes that precede fully-developed turbulent flow are large.

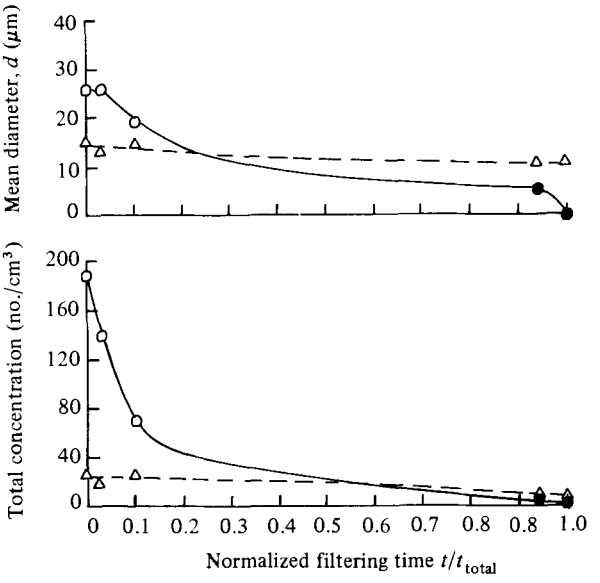

FIGURE 9. Variation of free-stream particulates and bubbles with bypass filtering time: ○, particles in the range 10 μm $\leqslant d \leqslant$ 70 μm; ●, particles in the range 1.6 μm $\leqslant d \leqslant$ 40 μm; △, bubbles in the range 9 μm $\leqslant d \leqslant$ 40 μm. $t_{total} = 4$ h.

4.2. *Water quality*

One of the objectives of this study is to establish a potential correlation between the amount of entrained particulate matter in the water and the transition Reynolds number of the body under various levels of surface heating. An effective way of doing this is to start out with relatively dirty water and then obtain transition data at selected intervals during a filtering process. The tunnel water (400 m^3 total volume) is drained and replaced with fresh water from a local well. This water is traditionally high in particulate matter and dissolved gas. Through use of the tunnel bypass system the particles and dissolved gas are removed, but the process requires several hours to reduce the levels significantly. Furthermore, the bypass operation can be stopped at any time and the facility operated in its routine manner while transition data are collected.

A history of the water quality, as measured in this programme, is given in figure 9. Here total concentration is defined as the total number of particles or bubbles measured without regard to size, per unit volume. Open circles denote those particles measured using the holographic technique, and the solid circles represent additional data acquired using the scanning-electron-microscope technique. Triangles are used to denote the free gas bubbles measured with the light-scattering method. The mean diameters of the particles and bubbles are also shown in figure 9 as functions of the filtering time. Transition data are obtained for each condition indicated by a datum point on this figure. It is emphasized that a given condition was maintained for as long a period as necessary in order to acquire the transition data.

The purest water considered occurs after several hours of filtering. The concentration of bubbles and particles are nearly equal at this condition, but very low; less than 10 cm^{-3}. Prior to this condition figure 9 shows that the water is dominated by particles, typically 20–26 μm in diameter.

Measured particle and bubble distributions are shown in figure 10. The cross-banded

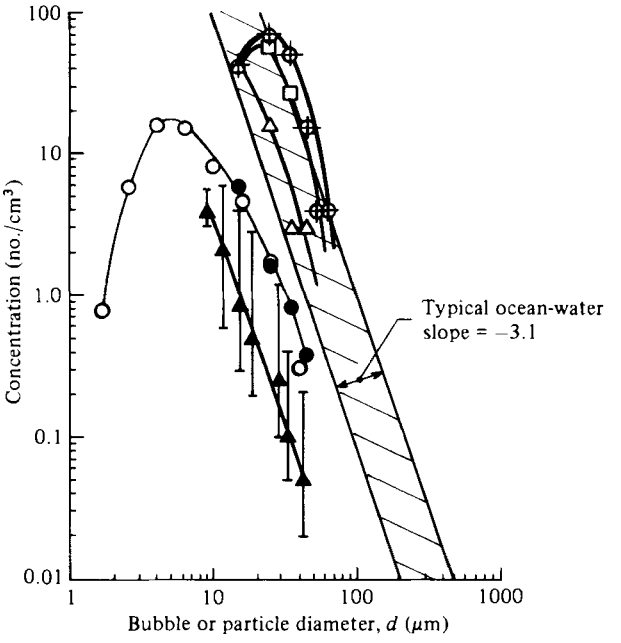

FIGURE 10. Particle- and bubble-size distributions measured during various phases of the experimental programme. For the particle data; ○, $t/t_{\text{total}} = 0.94$ (SEM measurement); ●, 0.94; △, 0.10; □, 0.03; ⊕, 0 (latter data measured with holographic technique). ▲, Bubbles measured with light-scattering technique; error bands are due to variations in velocity.

area of this figure represents the spread of typical particulate distributions measured in various oceans (Barker & Gile 1981). From this figure it is seen that the water-tunnel distributions considered fall below and within those of typical ocean water. Error bands are indicated for the bubble distributions because these measurements exhibit considerable scatter. The scatter is due to the dependence of bubble size on velocity.

4.3. *Baseline transition results*

In this subsection transition data are presented for the purest conditions of tunnel water ($t/t_{\text{total}} \geqslant 0.94$), where the aggregate concentration of particles and bubbles is less than 15 cm^{-3}. These data are considered baseline data and represent the best performance of the body. It is noted that the body was installed in the tunnel four different times during a 12 month time period, and that these baseline transition data were repeatable to within 5%. The data presented are for one hot-film probe only (located on the top of the body), because two of the three probes installed in the body did not perform satisfactorily.

Figures 11–14 show the baseline transition region statistical quantities γ and N as functions of the arclength Reynolds number. The transition Reynolds number is identified at $\gamma = 0.5$. The intermittency and burst-rate distributions are seen to broaden as the heating level (and transition Reynolds number) increases. Within the experimental scatter, no dependence of γ (or N) on whether u_0 is increasing or decreasing is observed. A hysteresis might be expected, however, if the integration time were decreased and the rate of velocity change increased. Such data could no longer be classed as steady-state, but as transient and would depend on the thermal inertia of the body itself.

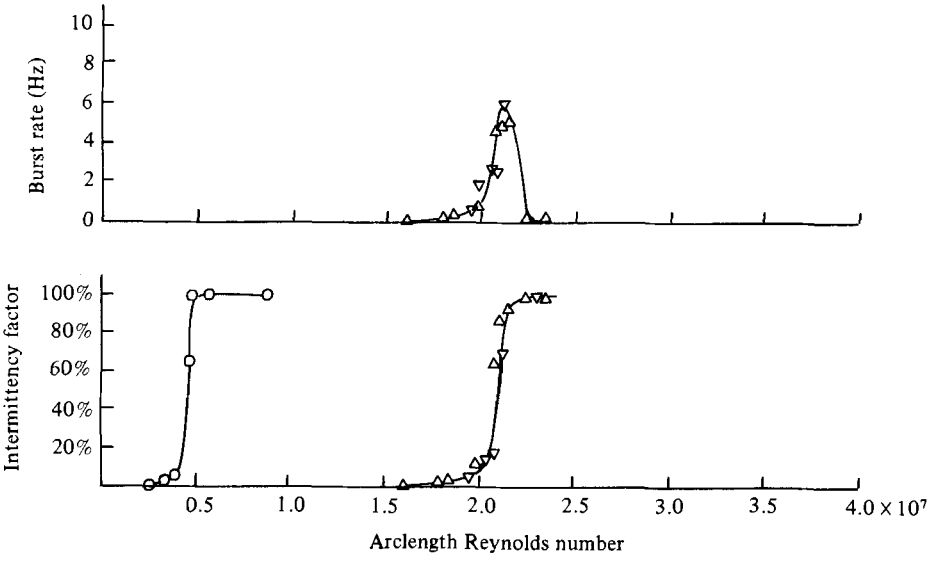

FIGURE 11. Variation of turbulence intermittency and burst rate with Reynolds number for baseline conditions and $Q_T = 26.6$ kW: ○, cold body; △, increasing u_0; ▽, decreasing u_0. $T_0 = 25.6$ °C (78 °F), $P_0 = 241.3$ kPa (35 p.s.i.a.), $\alpha_0 = 1.21$ p.p.m.

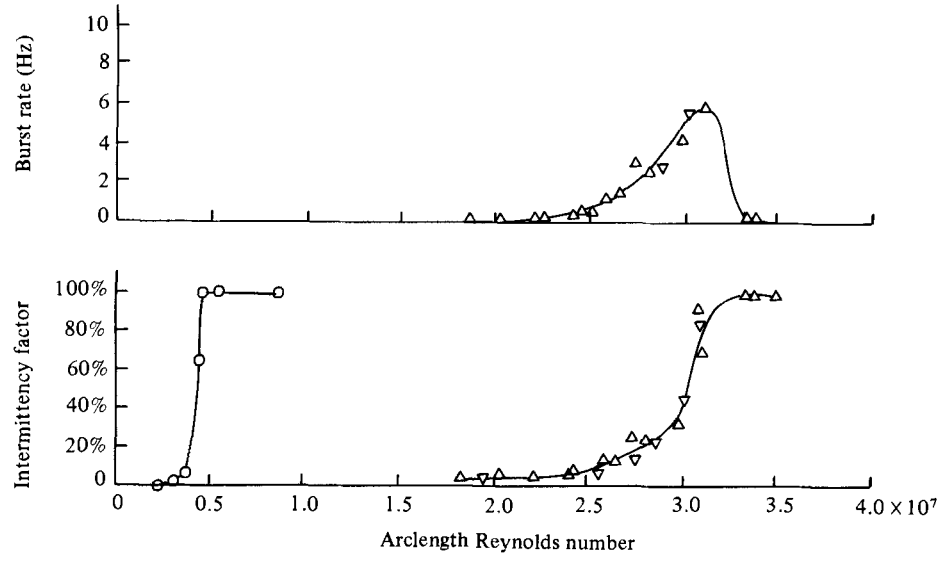

FIGURE 12. Variation of turbulence intermittency and burst rate with Reynolds number for baseline conditions and $Q_T = 53.4$ kW: ○, cold body; △, increasing u_0; ▽, decreasing u_0. $T_0 = 26.7$ °C (80 °F), $P_0 = 241.3$ kPa (35 p.s.i.a), $\alpha_0 = 1.21$ p.p.m.

The cold-body intermittency distribution is considered to be quasi-steady. With the hot-film probe situated at a relatively large arclength distance from the nose, the velocity must be set quite low ($u_0 \sim 1.5$ m/s) for laminar flow. At speeds lower than 3 m/s, the water velocity drifts, thus necessitating the collection of data over shorter time intervals. Nevertheless, the cold-body transition Reynolds number of 4.5×10^6 agrees well with that measured by other methods on another body of this size and shape (Lauchle *et al.* 1980).

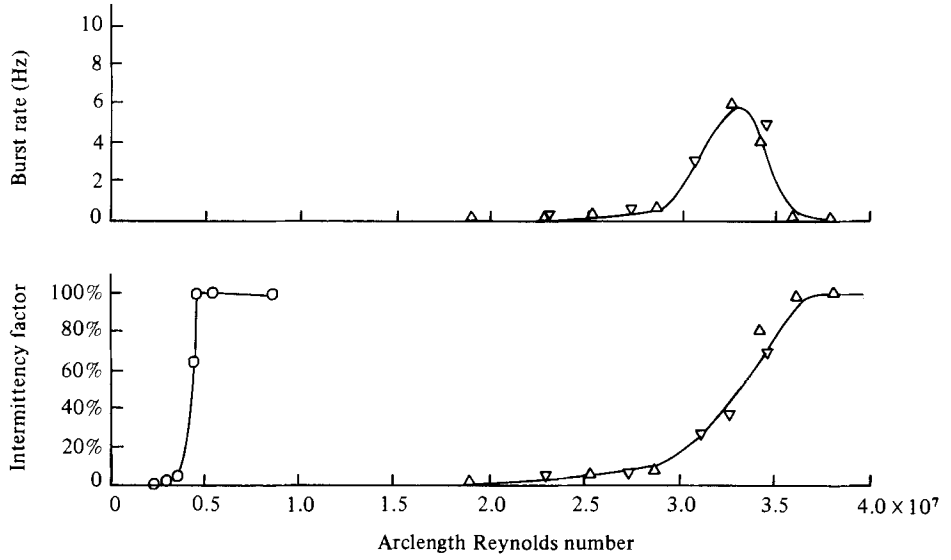

FIGURE 13. Variation of turbulence intermittency and burst rate with Reynolds number for baseline conditions and $Q_T = 75.4$ kW: ○, cold body; △, increasing u_0; ▽, decreasing u_0. $T_0 = 27.2$ °C (81 °F), $P_0 = 241.3$ kPa (35 p.s.i.a.), $\alpha_0 = 1.7$ p.p.m.

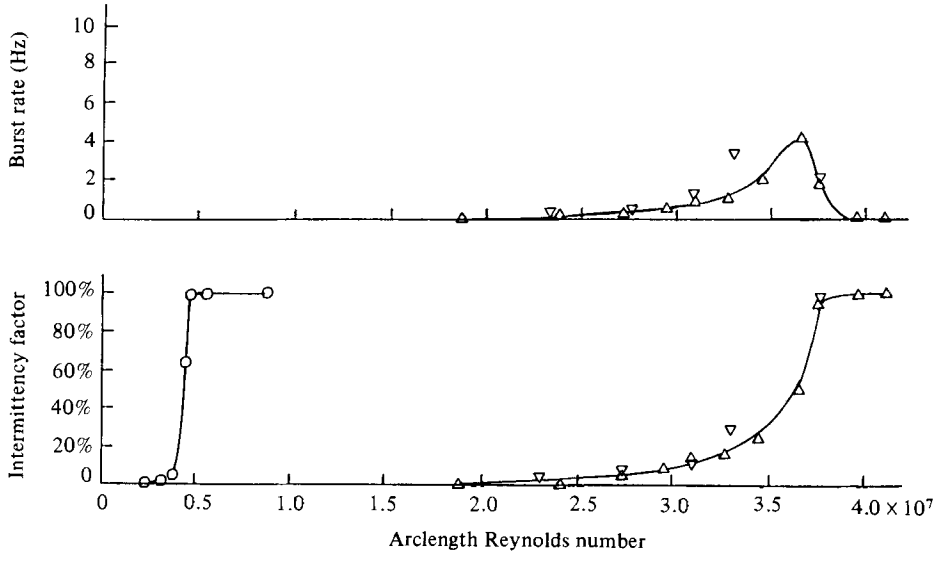

FIGURE 14. Variation of tubulence intermittency and burst rate with Reynolds number for baseline conditions and $Q_T = 93.3$ kW: ○, cold body; △, increasing u_0; ▽, decreasing u_0. $T_0 = 28.3$ °C (83 °F), $P_0 = 241.3$ kPa (35 p.s.i.a.), $\alpha_0 = 1.7$ p.p.m.

The heating distributions associated with the transition data of figures 11–14 are based on predictions that require the local displacement thickness Reynolds number to be less than a critical value $Re_{\delta^*\text{crit}}$. A given heat distribution should therefore provide enough heat to maintain full laminar flow over the body at the velocity noted for the prediction. A critical arclength Reynolds number can be defined as one based

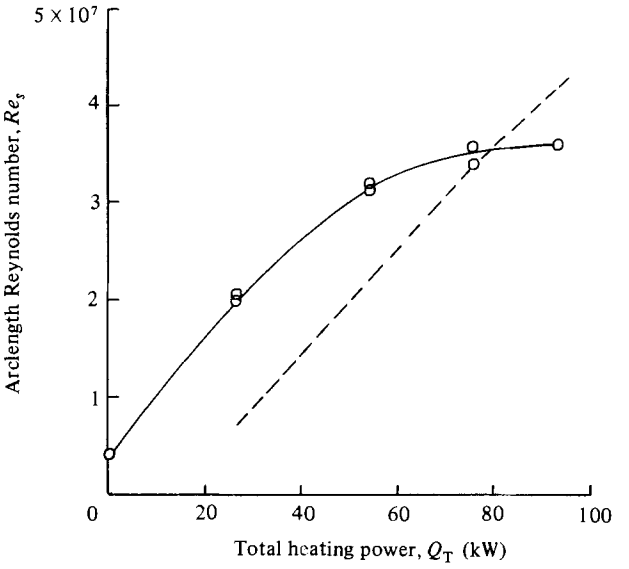

FIGURE 15. Comparison of experimentally determined transition Reynolds numbers with theoretical critical Reynolds numbers: ○, measured; – – –, theory.

on the velocity used in the heat prediction and on the arclength from the nose to the hot-film probe. A comparison of this critical Reynolds number with the measured transition Reynolds number is given in figure 15. One would expect the critical curve to fall substantially below the transition curve, as it does for the lower values of Q_T. However, for $Q_T > 60$ kW the two curves converge and cross. This behaviour is not inconsistent with what Barker & Gile (1981) observed for a heated-pipe flow. The theoretical methods used by Barker & Gile are analogous to those used here (Eisenhuth & Hoffman 1981). It is reasoned that for the higher Reynolds numbers (or higher heating levels), free-stream disturbances, surface flaws, flow asymmetries (buoyancy effects) and system idiosyncrasies become more important; their presence affects the measured results, but they are unaccounted for in the theoretical models.

The effects of thermal buoyancy forces on transition can be determined qualitatively from the work of Yao, Catton & McDonough (1980). They analyse the three-dimensional boundary layer over a heated semi-infinite cylinder of radius a and overheat ΔT. It is shown that a critical axial distance exists where the crossflow due to buoyancy forces decreases the axial velocity gradient on the top of the cylinder by a magnitude comparable to the increase in magnitude of the gradient due to local changes in viscosity created by heating. Thus, at this critical distance, one would anticipate that the effects of heating on boundary-layer stability would be diminished. The critical distance is $O(B\Delta T/\epsilon)^{\frac{1}{2}}$, where B is a constant arising from the viscosity ratio μ/μ_∞ and is given as 0.0272 $°C^{-1}$ by Yao *et al.* (1980). The parameter ϵ is the ratio of the Grashof number to the square of the Reynolds number, both based upon the maximum body radius a. The knee of the curve of figure 15 occurs where $\Delta T \sim 22$ °C and $u_0 \sim 14$ m/s. The critical axial distance is calculated to be $O(30$ m), ten times larger than the length of the body. Based on this result, it is unlikely that flow asymmetries due to thermal buoyancy contribute to the trends seen in figure 15.

The application of Emmons' (1951) spot theory allows one to express the burst

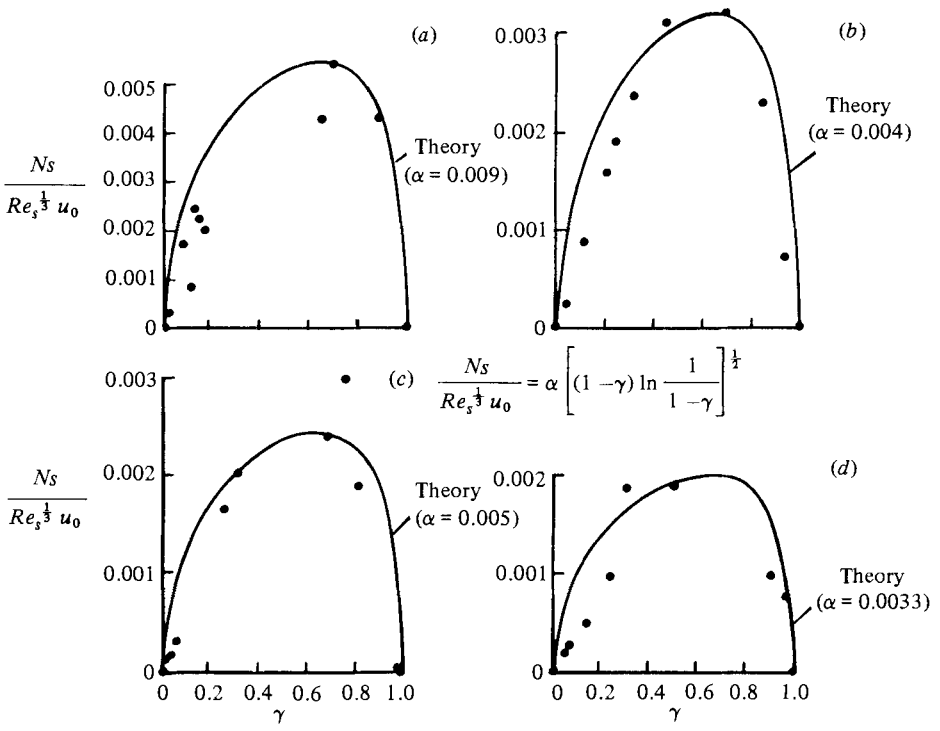

FIGURE 16. Non-dimensional burst-rate distributions for the baseline condition: (*a*) Q_T = 26.6 kW; (*b*) 53.4 kW; (*c*) 75.4 kW; (*d*) 93.3 kW. The constant α noted is used in (9) for each of the theoretical curves shown.

frequency in terms of the intermittency factor. Following Gedney (1979), a line-source density function is assumed, for which

$$\frac{N\Delta x}{u_0} \approx 4.76 \left[(1-\gamma) \ln \frac{1}{1-\gamma} \right]^{\frac{1}{2}}. \tag{7}$$

The streamwise extent of the transition zone is denoted by Δx. This length is not known for the present measurements, so it must be estimated. Chen & Thyson (1971) suggest that

$$Re_{\Delta x} \approx 60 Re_t^{\frac{2}{3}}, \tag{8}$$

where Re_t is the length Reynolds number where bursts first appear. Rearrangement of (7) using (8), and using the fact that $Re_s \sim Re_t$ ($s \equiv$ distance to the measurement probe) permits one to write

$$\frac{Ns}{Re_s^{\frac{1}{3}} u_0} = \alpha \left[(1-\gamma) \ln \frac{1}{1-\gamma} \right]^{\frac{1}{2}}, \tag{9}$$

where α is a proportionality constant.

Figure 16 shows the baseline non-dimensional burst rates as a function of intermittency factor for the four heating levels considered. The constant α of (9) is adjusted so that the theoretical curve matches the data. This matching reveals that α depends on Q_T in a nonlinear manner (figure 17). This dependence cannot be explained further until additional information is obtained on the behaviour of Δx

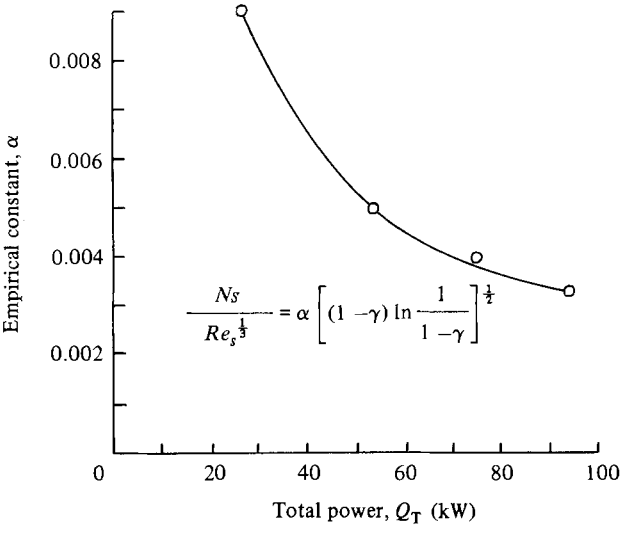

FIGURE 17. Variation of the empirical constant α of (9) with Q_T.

with varying levels of surface heating. (The constants in (7) and (8) are based on experiments with unheated walls.)

4.4 *Effect of increased particulate level*

With reference to figure 9, the baseline transition results of §4.3 are for normalized filtering times greater than 0.94. In this subsection transition data are presented for *much* shorter filtering times where the water is contaminated with high levels of particulate matter. Because the number of particles per unit volume is far greater than the number of observed bubbles, the particle concentration can be used as an independent variable.

Figure 18 shows the measured transition Reynolds numbers for the body operating at three different heating levels as a function of total particle concentration. Here total concentration is the total number of particles measured throughout the 10–70 μm diameter size range per unit volume of water. Figure 18 shows that the laminar-flow performance of the body degrades with increasing concentration of free-stream particulates. The effect seems to be progressively more important as the heating level increases. This is more easily seen by replotting the data as shown in figure 19. The transition Reynolds number is decreased by as much as 30 % owing to the introduction of the higher levels of free-stream particles.

The results given in figure 18 indicate that the decrease in transition Reynolds number with increasing particle concentration is a gradual dependence. The result is not unexpected, but explicit explanations for the mechanisms of instability due to free-stream particles or bubbles are difficult to formulate based on the current data (including those of Ladd & Hendricks 1982). The variables are many, and include particle size, particle concentration, boundary-layer thickness, heating level and particle relative velocity. Previous studies (e.g. Klebanoff, Schubauer & Tidstrom 1955; Hall 1967; and others) have investigated the effects of fixed spheres on transition. The current problem is similar, but more complicated owing to the additional variables associated with the particle motion relative to a heated surface. In this context one might class the previous work on three-dimensional protuberance-induced

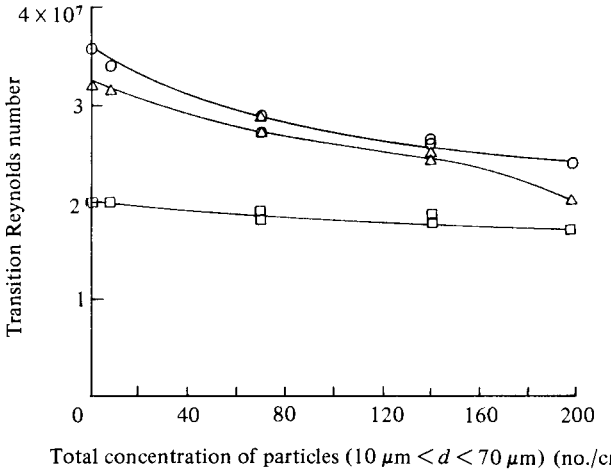

FIGURE 18. Variation of transition Reynolds number with concentration level of free-stream particles: □, $Q_T = 26.6$ kW; △, 53.4 kW; ○, 75.4 kW.

transition as a special case of particles that are free to move in and out of the boundary layer. As pointed out by Talbot *et al.* (1980), thermophoresis would be one possible mechanism that could cause particles to migrate toward a heated surface in a water flow. If this were to occur then the above-noted literature would become relevant. In addition, Hall (1967) showed that spheres placed within the inner 40 % of the laminar layer are effective in creating local turbulent events for sphere Reynolds numbers greater than about 500. This implies that a free-stream particle need not become attached to the surface in order to initiate local changes in vorticity which can lead to earlier transition.

Figure 19 indicates that the effect of particles on transition becomes more important as the heat level increases. Two possible effects may occur here. First, thermophoresis becomes more important as the overheat increases. This may cause more particles to contact the surface at high values of Q_T. Secondly, the displacement thickness δ^* decreases with increasing values of Q_T and Reynolds number. For a fixed band of particles the maximum particle diameter d_{max}, relative to δ^* would therefore increase. An increase in d_{max}/δ^* would presumably lead to increased laminar instability. These notions are qualitatively supported through observance that the cold-body transition Reynolds number is insensitive to the concentration of free-stream particles. For that condition ($Q_T = 0$) thermophoresis effects are absent. Based on calculations of δ^* at $s = 1.92$ m (just upstream of the transition probe) using the methods of Gentry & Wazzan (1976), it has been found that $d_{max}/\delta^* = 0.03$ for $Q_T = 0$, $d_{max} = 70$ μm and $u_0 = 1.22$ m/s (transition velocity). For comparative purposes, when $Q_T = 75.4$ kW and the transition velocity is 14.6 m/s, $d_{max}/\delta^* = 0.66$. At stations closer to the nose these ratios would, of course, be larger, but the marked difference between hot and cold would remain basically the same.

5. Conclusions

The present experimental investigation has shown that the transition Reynolds number can be significantly increased on a heated underwater body. The maximum transition Reynolds number achieved is 3.64×10^7, with an average overheat of 25 °C.

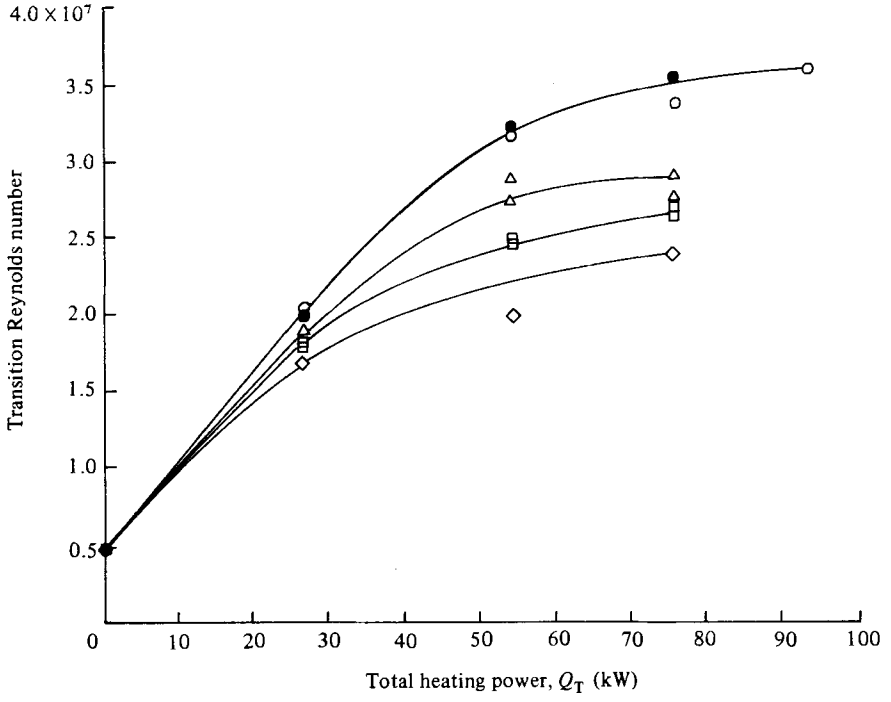

FIGURE 19. Variation of transition Reynolds number with total heating power supplied to the body: ●, less than 5 particles/cm³; ○, 9 particles/cm³; △, 70 particles/cm³; □, 140 particles/cm³; ◇, 198 particles/cm³. The size range of these particles is 10 μm ⩽ d ⩽ 70 μm.

The total heating power for this level of performance is 93.3 kW. The maximum Reynolds number can be compared with 4.5×10^6 for the body operating with no heat. Although higher heating levels were not considered, the results indicate that further increases in heating power would yield only marginal increases in the transition Reynolds number. For heating levels below 60 kW (average overheat 20 °C), the increase in transition Reynolds number with heat agrees well with theory. Above this level, the agreement is not good. A similar trend was observed for a heated-pipe flow (Barker & Gile 1981). This degradation in performance is attributed to free-stream disturbances, surface disturbances and system idiosyncrasies, none of which are accounted for in the theory, and none of which could be quantitatively determined in the context of these experiments.

Particles in the free stream are considered a free-stream disturbance that may lead to increased laminar instability. Their effect on the transition Reynolds number has been demonstrated in these experiments. The particles considered range from 10 to 70 μm in diameter. At high concentrations ($\sim$ 200 cm^{-3}) these particles decrease the transition Reynolds number by as much as 30 % at high heat levels. The degradation is less severe at lower heating levels. Because the transition Reynolds number increases monotonically with heating level, an alternative interpretation is that the instabilities created by a given size range of particles becomes progressively more severe as the particle-free (baseline) transition Reynolds number increases. This is an expected trend because the ratio of particle size to laminar boundary-layer thickness becomes larger at a fixed arclength as the Reynolds number increases. Also

at high heating levels, thermophoresis effects could cause more of the particles to migrate closer to the surface.

The decrease in transition Reynolds number with increasing concentration of particles is a gradually decreasing function. It is difficult therefore, to identify a critical concentration from which critical particle Reynolds numbers can be inferred. Additional work is necessary to identify these particle Reynolds numbers. The experiments are best performed at constant Reynolds number while various sizes of particles are introduced at a fixed concentration. Work is continuing in this area.

This work has been supported by the Applied Research Laboratory of The Pennsylvania State University under contract with the U.S. Naval Sea Systems Command, Code 63R-31. The staff of the Garfield Thomas Water Tunnel is acknowledged for help in performing this research program. Particular appreciation is extended to B. R. Parkin, S. Deutsch, F. H. Riedinger, G. D. Henderson, M. L. Billet, D. R. Stinebring and W. R. Hall. Also, discussions with Mark Morkovin and Eli Reshotko have been most useful in the interpretation of some of these results.

REFERENCES

BARKER, S. J. & GILE, D. 1981 *J. Fluid Mech.* **104**, 139.

BILLET, M. L. & GATES, E. M. 1981 *Trans. ASME.* I: *J. Fluids Engng* **103**, 8.

CHEN, C. P., GOLAND, Y. & RESHOTKO, E. 1979 Generation rate of turbulent patches in the laminar boundary layer of a submersible. In *Viscous Flow Drag Reduction* (ed. G. R. Hough), p. 73 (*Prog. Astro. Aero.* **72**).

CHEN, K. K. & THYSON, N. A. 1971 *AIAA J.* **9**, 821.

DAVIS, R. J. & BILLET, M. L. 1983 Light-scattering system: probe volume statistical analysis. In *Proc. ASME Cavitation and Multiphase Flow Forum, Houston, TX.*

EISENHUTH, J. J. & HOFFMAN, G. H. 1981 *J. Hydronaut.* **15**, 90.

EMMONS, H. W. 1951 *J. Aero. Sci.* **18**, 490.

FRICK, C. W. & MCCULLOUGH, C. B. 1942 Tests of a heated low drag airfoil. *NACA APR.*

GEDNEY, C. J. 1979 Wall pressure fluctuations during transition on a flat plate, *MIT Acoustics and Vibration Lab. Rep.* 84618–1.

GENTRY, A. E. & WAZZAN, A. R. 1976 The transition analysis program system. Vol. II – Program formulation and listings. *McDonnell Douglas Corp. Rep. MDC* J7255-02.

HALL, G. R. 1967 *AIAA J.* **5**, 1386.

KLEBANOFF, P. S., SHUBAUER, G. B. & TIDSTROM, K. D. 1955 *J. Aero. Sci.* **22**, 803.

LADD, D. M. & HENDRICKS, E. W. 1982 Effects of surface roughness and particulates on heated laminar flow. In *Proc. Appl. of LDAs to Fluid Mech., Portugal.*

LAUCHLE, G. C. 1979 *J. Hydronaut.* **13**, 61.

LAUCHLE, G. C. & CRUST, J. B. 1980 Particulate distributions in the Garfield Thomas 48-inch diameter water tunnel. *The Pennsylvania State University, Appl. Res. Lab. Rep.* TM 80–162.

LAUCHLE, G. C., EISENHUTH, J. J. & GURNEY, G. B. 1980 *J. Hydronaut.* **14**, 117.

LEHMAN, A. F. 1959 The Garfield Thomas Water Tunnel. *The Pennsylvania State University, Ordnance Res. Lab. Rep.* NOrd 16597–56.

LIEPMANN, H. W. & FILA, G. H. 1947 Investigations of effects of surface temperature and single roughness elements on boundary layer transition. *NACA Rep.* 890.

LOWELL, R. L. & RESHOTKO, E. 1974 Numerical study of the stability of a heated boundary layer. *Case Western Reserve University Rep.* FTAS/TR-73-95.

LUMLEY, J. L. & MCMAHON, J. F. 1967 *Trans. ASME. D: J. Basic Engng* **89**, 764.

RESHOTKO, E. 1976 *Ann. Rev. Fluid Mech.* **8**, 311.

RESHOTKO, E. 1978 Heated boundary layers. In *Proc. 12th Symp. on Naval Hydrodyn., Washington, DC*, p. 33.

ROBBINS, B. E. 1978 *J. Hydronaut.* **12**, 122.

STINEBRING, D. R. 1977 Unpublished manuscript.

STRAZISAR, A. J., RESHOTKO, E. & PRAHL, J. M. 1977 *J. Fluid Mech.* **83**, 225.

TALBOT, L., CHENG, R. K., SCHEFER, R. W. & WILLIS, D. R. 1980 *J. Fluid Mech.* **101**, 737.

WAZZAN, A. R., OKAMURA, T. T. & SMITH, A. M. O. 1968 *Trans. ASME* C: *J. Heat Transfer* **90**, 109.

WAZZAN, A. R., OKAMURA, T. T. & SMITH, A. M. O. 1970 The stability and transition of heated and cooled incompressible boundary layers. In *Proc. 4th. Intl Heat Transfer Conf., Paris.*

YAO, L.-S. 1977 Entry flow in a heated tube. *The Rand Corp., Santa Monica, CA., Rep.* R-2111-ARPA.

YAO, L.-S., CATTON, I. & MCDONOUGH, J. M. 1980 *J. Fluid Mech.* **98**, 417.